

# Genetic algorithm-based interpretation of shale core matrix-natural fracture parameters

Jian-Yi Liu<sup>1\*</sup>, Lu Jiang<sup>1</sup>, Shan Yi<sup>2</sup>, Miao Liu<sup>3</sup>, Zhi-Bin Liu<sup>1</sup>, Xue-Ni Dai<sup>1</sup>, Yi-Zhao Chen<sup>1</sup>, Yang Xie<sup>1</sup>

1 State Key Laboratory of Oil and Gas Reservoir Geology and Exploitation, Southwest Petroleum University, No.8 Xindu Ave, Chengdu, 610500, China

2 Southwest Oil and Gas Field Company, Petro-China, Chengdu, People's Republic of China.

3 Research Institute of Experimental and Detection, Petrochina Xinjiang Oilfield Company, Karamay, Xinjiang, 834000, China

## ABSTRACT

Shale pore-seepage parameters are the basic data for evaluating the seepage ability of shale formation. Due to the low-seepage characteristics of shale, only pulse attenuation method can be used to accurately test shale permeability. Various experimental results show that shale has distinct dual-pore characteristics, and conventional pulse attenuation method can only test the overall permeability and total porosity of shale. Based on the dual-hole characteristics of shale, this paper establishes a non-steady seepage model in shale matrix-natural cracks, solves it by Laplace transformation and fits it by genetic algorithm, and obtains an interpretation method for both shale matrix and natural fracture pore-seepage parameters by a set of data. This method can be used not only for the forward analysis of the pulse attenuation pressure response characteristics, but also for testing the pore and seepage parameters of natural fractures in shale core matrix by fitting experimental data. The correlation coefficients  $R^2$  of the two groups of experimental data were 0.9953 and 0.9996 respectively, and the fitting results were good.

**Keywords:** Genetic algorithm, Well Test interpretation, Shale Core, Permeability testing

## NONMENCLATURE

### Symbols

$C_g$	Gas Compression Factor in Core, $\text{Pa}^{-1}$
$C_{vp}$	Core Compression Factor, $\text{Pa}^{-1}$
$C_{v1}$	Upstream compression factor, $\text{Pa}^{-1}$
$C_{v2}$	Downstream compression factor, $\text{Pa}^{-1}$
$c_{tg}$	Gas Compression Factor, $\text{Pa}^{-1}$
$k_f$	Fracture permeability, $\text{m}^2$
$k_g$	gas permeability, $\text{m}^2$
$L$	Core length, m

Selection and peer-review under responsibility of the scientific committee of the 12th Int. Conf. on Applied Energy (ICAE2020).

Copyright © 2020 ICAE

$n$	Number of experimental data
$p_m$	Average pressure in core, Pa
$P_{ui}$	Upstream pressure calculated by the model, Pa
$P_{eui}$	Actual downstream pressure, Pa
$P_{di}$	Downstream pressure calculated by the model, Pa
$P_{edi}$	Actual downstream pressure, Pa
$q_f$	Fracture channeling to matrix per unit volume, $\text{kg}/(\text{m}^3 \cdot \text{s})$
$V_u$	Upstream bottle volume, $\text{m}^3$
$V_d$	Downstream bottle volume, $\text{m}^3$
$V_p$	Core Pore Volume, $\text{m}^3$
$V_1$	Upstream bottle volume, $\text{m}^3$
$V_2$	Downstream bottle volume, $\text{m}^3$
$\mu$	Gas Viscosity, $\text{mPa} \cdot \text{s}$
$\phi$	Core Porosity, decimal
$\rho_{gf}$	Gas density in cracks under experimental conditions, $\text{kg}/\text{m}^3$
$\rho_{gsc}$	Gas Density Under Ground Standard Conditions, $\text{kg}/\text{m}^3$
$v_{gf}$	Gas flow rate in cracks, $\text{m}/\text{s}$
$\phi_f$	Fracture Pore Volume, $\text{m}^3$
$\rho_{gm}$	Gas Density at Mean Pressure, $\text{kg}/\text{m}^3$
$\phi_m$	Matrix Pore Volume, $\text{m}^3$

## 1. INTRODUCTION

At present, the methods used for core permeability testing are mainly divided into steady state and non-steady state methods. Because of the extremely dense nature of shale, the steady-state method has a large error in testing the permeability of dense cores and a long test time because it cannot accurately judge the time to reach the steady state or test the fluid flow accurately.

In the 1960s, Brace<sup>[1]</sup> first established a non-steady-state permeability test method for dense granite. This method establishes the pulse attenuation in cores based on the elastic hypothesis. It tests the core permeability by testing the upstream and downstream pressure response. For dense cores, it is easier to test the pressure change than to test the flow rate, so the pulse attenuation method is superior to the steady-state method. Next, many researchers have improved the experimental method<sup>[7]</sup> and the solution method<sup>[8]</sup> based on the pulse decay method established by Brace.

Shale has distinct dual media characteristics<sup>[3][10]</sup>. Shale core seepage model under dual media conditions is different from that of conventional cores<sup>[5]</sup>. In recent years, some scholars have established dual media pulse attenuation model<sup>[4][6]</sup> for Shale Based on dual pore characteristics of shale, but these studies can not explain the pore seepage parameters of matrix and natural cracks, so it is necessary to establish a dual pore model. Test method for pore and seepage parameters of matrix and natural fractures.

On the basis of previous research, this paper establishes a pulse attenuation model to characterize the dual-hole characteristics of shale, and obtains the analytical solution of pressure response in pull-down space by Laplace transformation. Combining with numerical inversion and genetic algorithm, a method for simultaneous test and analysis of shale matrix and fracture flow parameters is established. This method can not only forward analyze the dual-hole characteristics of shale pulse attenuation pressure curve. It can also be used to fit test data to interpret pore and seepage parameters of shale matrix and natural fractures.

## 2. PULSE ATTENUATION MODEL OF POROUS MEDIA

### 2.1 Gas flow model in two porous media

The gas flow model in the upstream and downstream systems is as follows:

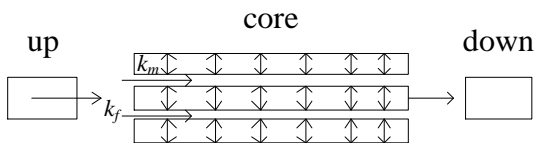


Fig. 1 Schematic diagram of double hole seepage in rock core Under the action of pressure difference, the gas enters the downstream bottle through the core natural fracture through the upstream bottle, and the gas in the natural fracture will also flow into the matrix. When the adsorbable gas such as CH<sub>4</sub> is selected as the test gas, the gas flow model considering adsorption and desorption in

the double porous medium model can be described by the following equation:

$$\frac{\partial(\rho_{gm} v_{gm})}{\partial x} + q_f = \frac{\partial(\phi_m \rho_{gm})}{\partial t} + \rho_{gsc} \frac{\partial V_E}{\partial t} \quad (2-1)$$

$$\frac{\partial(\rho_{gf} v_{gf})}{\partial x} - q_f = \frac{\partial(\phi_f \rho_{gf})}{\partial t}$$

In this paper, the channeling flow from fracture to matrix is expressed as unsteady channeling flow. Assuming that the matrix block is round and spherical, under the spherical coordinates, there are:

$$\frac{1}{r^2} \frac{\partial}{\partial r} \left( r^2 \frac{\partial p_m}{\partial r} \right) = \frac{\phi_m \mu_m c_m}{k_m} \frac{\partial p_m}{\partial t}$$

$$\left. \frac{\partial p_m}{\partial r} \right|_{r=0} = 0$$

$$p_m(r, t) \Big|_{r=r_1} = p_f$$

$$q_f = - \frac{3 k_m}{r_1 \mu} \left. \frac{\partial p_m}{\partial r} \right|_{r=r_1}$$

The pseudo pressure and dimensionless parameters are defined:

The pseudo pressure is as follows:

$$\psi_{u,d,m,f} = 2 \int_{p(u,d,m,f)_0}^{p_{u,d,m,f}} \frac{P_{u,d,m,f}}{\mu_{u,d,m,f} Z_{u,d,m,f}} dp_{u,d,m,f} \quad (2-3)$$

Where u, D, m and F are upstream, downstream, matrix and fracture, respectively.

Dimensionless pressure was as follows:

$$\psi_{Dj} = \frac{\psi_j - \psi_{d0}}{\psi_{u0} - \psi_{d0}}, \quad j = u, d, m, f \quad (2-4)$$

The other dimensionless parameters are as follows:

$$t_D = \frac{k_f t}{\mu(\phi_f c_f + \phi_m c_{ig}) L^2}, X = \frac{x}{L}, \omega = \frac{\phi_f c_f}{\phi_f c_f + \phi_m c_{ig}} \quad (2-5)$$

$$c_{ig} = c_m + \frac{\rho_{gsc} V_L P_L}{\rho_{gm} \phi_m (P_L + p_m)^2}, r_D = \frac{r}{r_1}$$

The dimensionless channeling coefficient and matrix shape factor are expressed as follows:

$$\lambda = \alpha L^2 \frac{k_m}{k_f}, \alpha = \frac{15}{r_1^2} \quad (2-6)$$

Then, formula 3-2 can be written as follows:

$$\frac{\partial \psi_{Dm}}{\partial r_D} + \frac{2}{r_D} \frac{\partial \psi_{Dm}}{\partial r_D} = \frac{15(1-\omega)}{\lambda} \frac{\partial \psi_{Dm}}{\partial t}$$

$$\left. \frac{\partial \psi_{Dm}}{\partial r_D} \right|_{r_D=0} = 0$$

$$\psi_{Dm}(r_D, t_D) \Big|_{r_D=1} = \psi_{Df}$$

In the pull space, the following solutions are obtained:

$$\left. \frac{\partial \overline{\psi_{Dm}}}{\partial r_D} \right|_{r_D=1} = (W \coth W - 1) \overline{\psi_{Df}} \quad (2-8)$$

$$W^2 = \frac{15(1-\omega)s}{\lambda} \quad (2-9)$$

The fracture equation is as follows:

$$\begin{aligned} \frac{\partial^2 \overline{\psi}_{Df}}{\partial X^2} &= sf(s) \overline{\psi}_{Df} \\ \overline{\psi}_{Df}(0, t_D) &= \overline{\psi}_{Du}(t_D) \\ \overline{\psi}_{Df}(1, t_D) &= \overline{\psi}_{Dd}(t_D) \end{aligned} \quad (2-10)$$

By solving the above equations, the following results are obtained:

$$\overline{\psi}_{Df} = \frac{\overline{\psi}_{Dd} - e^{-\sqrt{sf(s)}} \overline{\psi}_{Du}}{2sh\sqrt{sf(s)}} e^{\sqrt{sf(s)}X} + \frac{-\overline{\psi}_{Dd} + e^{\sqrt{sf(s)}} \overline{\psi}_{Du}}{2sh\sqrt{sf(s)}} e^{-\sqrt{sf(s)}X} \quad (2-11)$$

$$f(s) = \omega + \frac{\lambda}{5s} \left[ \sqrt{\frac{15(1-\omega)s}{\lambda}} \coth \left( \sqrt{\frac{15(1-\omega)s}{\lambda}} - 1 \right) \right] \quad (2-12)$$

## 2.2 pstream and downstream bottle equation

Through the above flow model, we can get the following results:

For upstream bottles:

$$\rho_{fg} v_{fg} A = \frac{\partial}{\partial t} (\rho_u V_u) \quad (2-13)$$

For downstream bottles:

$$\rho_{fg} v_{fg} A = -\frac{\partial}{\partial t} (\rho_d V_d) \quad (2-14)$$

In the same way, we can get the following results:

$$\begin{aligned} \left[ \frac{\partial \overline{\psi}_{Df}}{\partial X} \right]_{x=0} &= -A_u \frac{\partial \overline{\psi}_{Du}}{\partial t_D} \\ \left[ \frac{\partial \overline{\psi}_{Df}}{\partial X} \right]_{x=1} &= A_d \frac{\partial \overline{\psi}_{Dd}}{\partial t_D} \end{aligned} \quad (2-15)$$

$$A_u = \frac{V_u c_{tu}}{A \phi_f (\phi_f c_f + \phi_m c_{ig}) c_{ig} L} \quad (2-16)$$

$$A_d = \frac{V_d c_{td}}{A \phi_f (\phi_f c_f + \phi_m c_{ig}) c_{ig} L}$$

In the pull space, the analytical solution of the upstream and downstream pressure response can be obtained by combining the fracture equation and the upstream and downstream bottle equations

$$\begin{aligned} \overline{\psi}_{Dd} &= \frac{\sqrt{sf(s)} A_u}{sh\sqrt{sf(s)}} \frac{A_u}{\left( \frac{\sqrt{sf(s)}}{th\sqrt{sf(s)}} + A_u s \right) \left( \frac{\sqrt{sf(s)}}{th\sqrt{sf(s)}} + A_d s \right) - \left( \frac{\sqrt{sf(s)}}{sh\sqrt{sf(s)}} \right)^2} \\ \overline{\psi}_{Du} &= \frac{\left( \frac{\sqrt{sf(s)}}{th\sqrt{sf(s)}} + A_d s \right) A_u}{\left( \frac{\sqrt{sf(s)}}{th\sqrt{sf(s)}} + A_u s \right) \left( \frac{\sqrt{sf(s)}}{th\sqrt{sf(s)}} + A_d s \right) - \left( \frac{\sqrt{sf(s)}}{sh\sqrt{sf(s)}} \right)^2} \end{aligned} \quad (2-17)$$

## 3. MODEL RESULTS AND ANALYSIS

In this paper, the dimensionless parameters are inversely calculated to the real parameters, and the influence of each real parameter on the pulse

attenuation curve is analyzed, which makes the analysis more intuitive and accurate.

Some scholars have analyzed the characteristics of pressure response curve under dual pore characteristics, and also analyzed the influence of dimensionless parameters on the pressure response curve. This paper mainly analyzes the influence of core basic parameters, container parameters and adsorption desorption on the pressure response curve.

### 3.1 Matrix permeability

The relevant parameters used to analyze the influence of matrix permeability on pressure response curve are shown in table, and the calculation results are shown in figure. From the pressure response curve, we divide the pulse attenuation pressure response curve under the characteristics of double holes into two stages: the upstream pressure decreases in the first section, and the downstream pressure increases until the upstream and downstream pressures are equal; in the second stage, the upstream and downstream pressures decrease simultaneously until no change is made. It can be seen that matrix permeability has little effect on the first section, but mainly affects the second section. The smaller the matrix permeability is. The longer the second segment, the longer it takes to reach the final equilibrium.

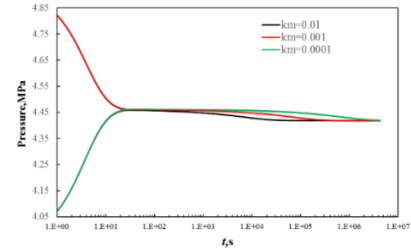


Fig. 3-1 Pulse attenuation curves of different matrix permeability

### 3.2 Natural fracture permeability

The relevant parameters used to analyze the influence of natural fracture permeability on pressure response curve are shown in table, and the calculation results are shown in figure. It can be seen from the figure that the fracture permeability mainly affects the first section. The smaller the natural fracture permeability is, the longer the first section is, and the longer it takes to reach the first pressure balance. Combined with the influence characteristics of fracture permeability, the first section of pulse attenuation pressure response curve can be considered that the fracture flow section is mainly affected by natural fracture permeability, and the

second section is matrix flow section, which is mainly affected by matrix permeability.

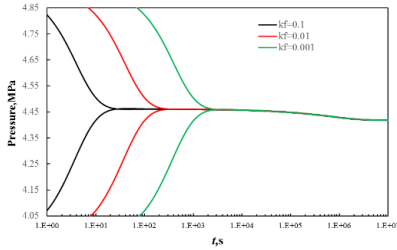


Fig. 3-2 Pulse attenuation curves of different fracture permeability

### 3.3 Volume of upstream and downstream bottles

The relevant parameters used to analyze the influence of matrix permeability on pressure response curve are shown in table, and the calculation results are shown in figure. The volume of upstream and downstream bottles has a great influence on the pulse attenuation pressure response curve, especially in the matrix flow section. The larger the volume of upstream and downstream bottles, the less obvious the matrix flow section. However, in the experimental test, if the volume of upstream and downstream bottles is too small, the first section of pressure response curve will drop too fast, and the pressure sensor can not accurately test. Considering the actual test accuracy and the accurate measurement of matrix flow section, it is necessary to make the upstream and downstream bottle volume close to the pore volume.

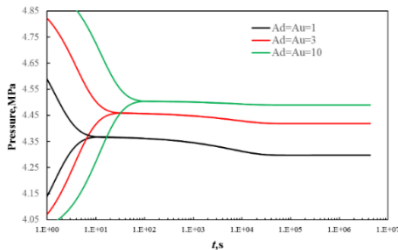


Fig. 4-3 Pulse attenuation curves of different combinations of upstream and downstream bottles permeability

### 3.4 Adsorption and desorption

It can be seen from the figure that the pressure response curves with and without adsorption effect are not very different. The adsorption desorption phenomenon mainly affects the final equilibrium pressure, and the influence of adsorption and desorption is relatively small. The equilibrium pressure considering adsorption and desorption is reduced by 0.2136%.

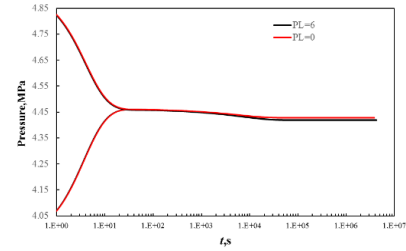


Fig. 3-4 Effect of adsorption and desorption on pulse attenuation curve

### 3.5 Example calculation and result analysis

In this paper, the pulse attenuation test data of Barnett shale core by Cronin (2014)<sup>[9]</sup> and the experimental data of independent pulse attenuation method using CH<sub>4</sub> as carrier gas are fitted and calculated, so as to verify the applicability of the method. The experimental data are related to the Cronin (2014) test data, and the rock core and equipment parameters are shown in the table below:

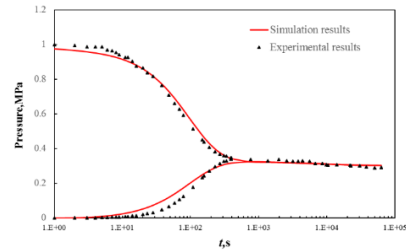


Fig 3-5 Independent experimental data and fitting results  
Table 3-5 Experimental parameters

	Independent experiment	Cronin (2014)
$L, 10^{-2}m$	5.308	1.764
$D, 10^{-2}m$	2.482	3.784
$V_1, 10^{-6}m^3$	2.112	2.120
$V_2, 10^{-6}m^3$	3.901	1.763
$T, K$	300.95	303.15

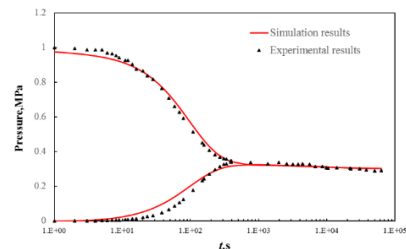


Fig. 3-6 Cronin (2014) experimental data and fitting results  
Table 3-6 Explain the results

	Independent experiment	Cronin (2014)	
	this paper	Cronin (2014)	this paper

$K_f, 10^{-15} \text{m}^2$	$3.046 \times 10^{-2}$	$9.2 \times 10^{-5}$	$1.01 \times 10^{-4}$
$K_m, 10^{-15} \text{m}^2$	$5.138 \times 10^{-6}$	$2.3 \times 10^{-6}$	$2.69 \times 10^{-6}$
$\phi_m, \%$	4.345		5.4
$\phi_f, \%$	1.337	6.9	0.878

In this paper, the correlation coefficient of interpretation results of self-test experimental data is  $R^2 = 0.9953$ , and the correlation coefficient of interpretation results of Cronin (2014) experimental data is  $R^2 = 0.9996$ . The method proposed in this paper can simultaneously interpret the pore permeability parameters of shale matrix and natural fractures according to a set of experimental data of pulse attenuation method, which provides data support for understanding the physical parameters of shale dual porosity characteristics.

### 3.6 Conclusions

In this paper, the core flow equation of shale dual porosity medium is solved by Laplace transform, and the test data are fitted by genetic algorithm. The test method of porosity and permeability parameters for shale matrix and natural fracture is established simultaneously. The applicability and accuracy of the method were verified by the comparison of experimental test and fitting results.

1. The pulse attenuation process of double porosity shale can be divided into fracture seepage section affected by fracture permeability and matrix seepage section affected by matrix permeability;

2. Considering the actual measurement accuracy, in order to accurately test matrix permeability, it is necessary to make the upstream and downstream bottle volume close to the core pore volume as far as possible;

3. In the pulse attenuation method, the effect of adsorption and desorption can reduce the equilibrium pressure by 0.2136%.

Compared with the previous experimental results, the fitting accuracy of this method is 0.9953 and 0.9996 respectively. The fitting accuracy is higher, and the fitting results can also confirm with the previous scholars' fitting results. Compared with the previous test methods, this method can fit the porosity and permeability parameters of matrix and natural fracture respectively.

### ACKNOWLEDGEMENT

This work was supported by the National Science and Technology Major Project (Grant No. 2016ZX05053).

### REFERENCE

[1]Brace, W.F., Walsh, J.B., Frangos, W.T., 1968. Permeability of granite under high pressure. *J. Geophys. Res.* 73 (6), 2225–2236.

[2]Dicker A, Smits R. A practical approach for determining permeability from laboratory pressure-pulse decay measurements[C]. International meeting on petroleum engineering, 1988.

[3]D.J. Ross, R.M. Bustin The importance of shale composition and pore structure upon gas storage potential of shale gas reservoirs *Mar. Pet. Geol.*, 26 (6) (2009), pp. 916-927

[4]Guofeng Han, Liang Sun, Yuewu Liu, Shangwen Zhou, Analysis method of pulse decay tests for dual-porosity cores, *Journal of Natural Gas Science and Engineering*, Volume 59, 2018, Pages 274-286

[5]Hudson, J.D., 2011. Quad-porosity Model for Description of Transport in Shale-gas Reservoirs. University of Oklahoma, USA (Master thesis).

[6]Huangye Chen, Hui-Hai Liu, Pressure pulse-decay tests in a dual-continuum medium: An improved technique to estimate flow parameters, *Journal of Natural Gas Science and Engineering*, Volume 65, 2019, Pages 16-24

[7]Jones, S.C., 1997. A technique for faster pulse-decay permeability measurements in tight rocks. *SPE Form. Eval.* 12 (1), 19–25.

[8]Lin, 1977 W. Lin Compressible Fluid Flow Through Rocks of Variable Permeability (1977) Google Scholar

[9]M.B. Cronin Core-scale Heterogeneity and Dual-permeability Pore Structure in the Barnett Shale The University of Texas at Austin, USA (2014) PhD thesis

[10]R.J. Ambrose, R.C. Hartman, M. Diaz-Campos, I.Y. Akkutlu, C.H. Sondergeld Shale Gas-in-Place Calculations Part I: New Pore-Scale Considerations *SPE J.*, 17 (1) (2012), pp. 219-229